

Monitoring of supporting structures with profile laser scanning

Florian Schill¹, Andreas Eichhorn

Received: September 2018 / Accepted: October 2018 / Published: December 2018
© Journal of Geodesy, Cartography and Cadastre/ UGR

Abstract

This paper presents the evaluation of measurements on bridge structures with a profile scanner and shows that existing concepts of classical monitoring measurements can be extended with the use of profile laser scanning.

The contact-free acquisition method of profile laser scanners reduces the expense for personnel and instrumentation compared to conventional sensors used for the monitoring of civil engineering structures. It furthermore enables the measurement of non-accessible areas of the monitored supporting structures. In addition, the availability of information along an entire structural profile can be used to flexibly deal with a wide variety of problems. With a measurement rate of at least 50 Hz, typical structural deformation signals can be recorded and sufficient data can be collected to characterize the underlying deformation processes dependably.

Overall, an automated and efficient spatio temporal processing scheme is presented, which is based on the discrete wavelet transform. With this signal analysis tool outliers are detected and eliminated, but furthermore an automated structural analysis based on the details of the supporting structures surface is realized.

In addition to the derivation of deformations, a quality assessment with comprehensive integration of the redundant measurement information is possible as an in-situ uncertainty determination.

Keywords

Laser scanning, discrete wavelet transform, monitoring, supporting structures, bridges, time series analysis, spatio temporal processing scheme

1. Motivation

A fundamental objective of geodetic monitoring is the acquisition of geometric object changes under the influence of loads [1]. In particular, the monitoring of supporting structures is of great importance, since the structural members as a whole system of all supporting elements of a construction or engineering structure are responsible for its stability.

Since engineering structures are often systems that are capable of vibration and the predominant part of all load factors has a dynamic character, the focus of corresponding monitoring measurements is on the collection of temporally variable structural deformations. These deformations can only be recorded with sensors that provide a high temporal resolution.

Up-to-date the primary components of such measuring concepts are acceleration sensors, inductive displacement sensors and strain gauges. Although these sensors provide highly accurate data that is optimally adapted to the application, they must be mounted on the measuring object producing an enormous workload. Furthermore, inaccessible areas that do not allow the mounting of these sensors are particularly problematic. In general, the measurement information obtained in this way is only available at discrete object points and cannot be interpreted without appropriate prior knowledge about the supporting structure.

The purpose of this paper is to demonstrate that profile scanners have the potential to solve the problems discussed above and to complement existing measurement concepts. Due to the repeated acquisition along a profile, the measurement data possesses both temporal and spatial resolution, which can be ideally combined with the measurement information obtained at discrete points.

In the following chapter the measurement system is introduced and the most important parameters are explained.

Chapter 3 shows how the derivative of spatially distributed time series is carried out in the context of space-temporal processing using the temporal and spatial resolution of the profile scanner.

¹ Dr.-Ing. Florian Schill
Technische Universität Darmstadt
FG Geodätische Messsysteme und Sensorik
Institut für Geodäsie
Franziska-Braun-Straße 7
64287 Darmstadt
schill@geod.tu-darmstadt.de

The basic principles are further deepened with practical examples in Chapter 4 and 5. The main focus lies on railway bridges, whereby the examples differ significantly in the deformation signals and bridge characteristics that occur. This shows the potential of the profile scanner for the monitoring of supporting structures and demonstrates the universal applicability of the developed processing scheme.

2. Measurement system based on a profile scanner

The profile scanner used in this investigation is a phase-based Zoller+Fröhlich Profiler 9012. It is a pure 2D scanner, see Figure 1. All adapters for using it in the area of monitoring are proprietary developments (tripod and targeting adaptor). Due to the special type of adaptation both vertical and horizontal measurements are possible, but also in the entire angle range in between. Since the profile scanner is equipped with a GPS receiver, a time stamp can be calculated for each individual point. The maximum measurement distance is specified by the manufacturer with 119 m. With a data recording rate of up to 1 million points per second, measuring speeds of 50, 100 or 200 profiles per second are possible [2].



Fig. 1 Profile scanner under a railway bridge.

In Figure 1, a schematic measurement profile and the corresponding coordinate axes are displayed together with the profile scanner. Accordingly, Figure 2 shows the y-/z-measurement plane of the profile scanner with approximately 20.000 measuring points in one measurement profile.

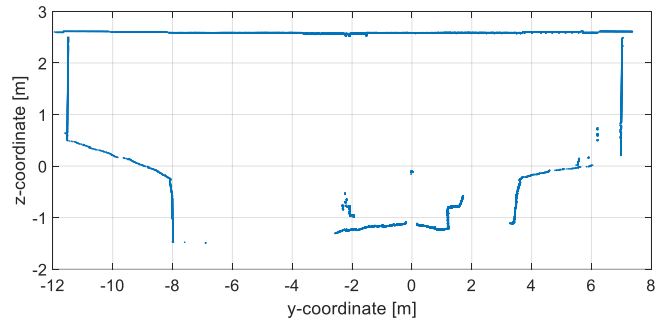


Fig. 2 Raw measurement profile with approximately 20.000 points.

3. Spatio temporal processing scheme

The profile scanner determines a spatial and temporal component for every measured point, which corresponds to a spatio temporal acquisition of the structural members. However, the original measured values of the profile scanner are not directly usable for the monitoring of supporting structures, as they are not directly accessible and on the other hand not reproducible [3].

The measured values (organized in profiles) must therefore be analyzed in the context of the structural surface and local conditions. Due to the large number of measurement profiles belonging to a scan, this analysis has to be automated for efficiency reasons.

For this purpose, a universally applicable processing scheme has been developed, of which the flowchart is depicted in Figure 3. The scheme subdivides into three parts:

- The automatic analysis of the measurement profiles,
- The profile-wise spatial processing,
- The scan-wise temporal processing.

The first step is the **automatic analysis of the measurement profiles** with the objective to eliminate all measured points not belonging to the structural surface and to segment the complex measurement profiles into simpler segments. This part of the spatio temporal processing scheme is presented in detail in [3] and [4].

Based on those simplified profile segments a **profile-wise spatial processing** can be implemented for example as an approximation with spatial clustering, B-spline functions [5], wavelets [6] or others. Those spatial processing approaches are extensively discussed in [3].

The choice of the different processing approaches depends heavily on the structure to be examined. In principle, it can be differentiated into two categories: smooth surfaces, as in the investigations of wind turbines in [7] or structured object surfaces, which can occur at steel bridge structures [4].

In case of smooth surfaces, the selection of the evaluation strategy is relatively free and depends mainly on the evaluation target, such as the use of continuous functions for the determination of eigenmodes or the formation of spatial cluster for the calculation of eigenfrequencies of the supporting structure.

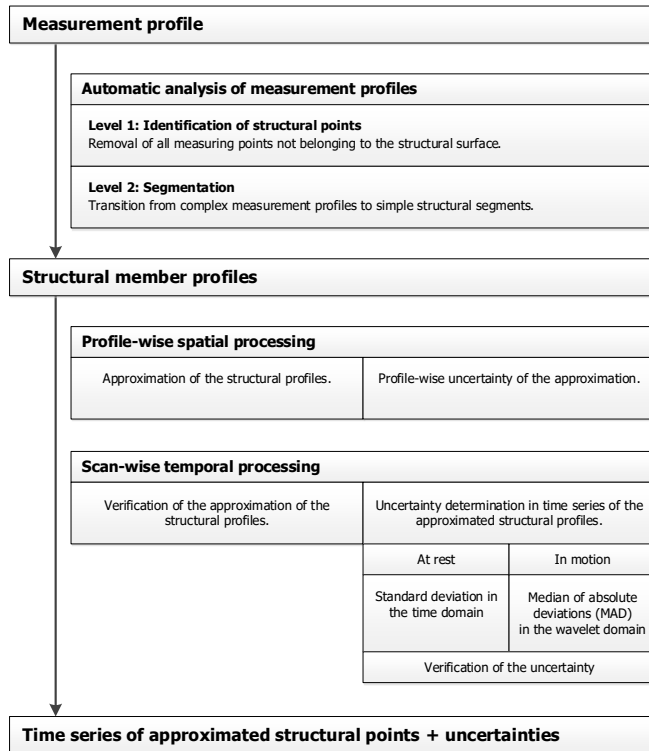


Fig. 3 Spatio temporal processing scheme.

Independent of the profile-wise spatial processing method, after the following **scan-wise temporal processing**, the final results are time series of approximated structural points and corresponding uncertainties. These can be used as a starting point for investigations that optimally capture the deformation behavior both in terms of space and time, thus forming the basis for the monitoring of supporting structures with a profile scanner.

In the following the application of the spatio temporal processing scheme will be reviewed in detail with two very different examples, which vary not only in the before mentioned difference of the supporting structures surface, but also in the occurring deformation signals:

- **Example 1:** A steel bridge with a heavily structured surface (Chapter 4) whereas the analysis concentrates on quasi static deformations.
- **Example 2:** A steel bridge with a smooth surface (Chapter 5) whereas the analysis concentrates on the dynamic deformation component.

4. Example 1: Single-tracked railway bridge over the Flanitz at Klingenbrunn

The examined engineering structure is an over one hundred year old single-tracked railway bridge with a span of just under 20 m. The main beams are designed as solid steel girders and only sit on the two abutments, see Figure 4. The bridge was subsequently extended by two footpaths, which are connected with the actual bridge only at the abutments.



Fig. 4 Side view of the single-tracked railway bridge.

The measurements took place during ongoing railway operations. The trains were Regio-shuttle RS1 with an empty weight of approx. 41 tones and a speed at the bridge crossing of approx. 30 km/h. The individual passages are therefore distinguished mainly by the direction of travel and the number of used wagons.

With the profile scanner two different measurement configurations have been recorded which will be reviewed in the following:

- Along the bridge axis on the main girders (4.1),
- Perpendicular to the bridge axis in the middle of the bridge (4.2).

4.1 Analysis of the main girders along the bridge axis

Figure 5 shows a schematic longitudinal section through the bridge structure along one main girder. Since the two main girders are identical in construction, this figure is representative for both of them. The main girders consist of two steel full-wall beams, which are connected in the middle of the bridge. To connect and stabilize the two parts of the main girders they are additionally stiffened to the middle of the bridge. This is greatly exaggerated in Figure 5 by the increasing thickness of the main girder.

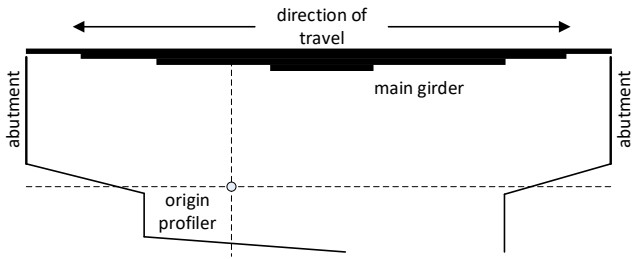


Fig. 5 Schematic longitudinal section through the main girder of the single-tracked railway bridge.

In Figure 6 the result of the automatic analysis of an exemplary measurement profile is shown for the first configuration. According to the statements of Chapter 3, the automatic analysis of the measurement profiles removes erroneous measurements as well as disturbing structural details. Following this, the structure of the surface is segmented based on its details. In Figure 6 the measurement points belonging to the resulting structural segments are highlighted in color from the original profile measurement (in blue). In this case, the surface structure of the main girder leads to a segmentation into eight parts.

The results of the automatic analysis of the measuring profiles are so-called structural segments, which have to be further processed for the spatio temporal determination of the vertical deformation, see Figure 3. In this case an approximation with continuous functions such as B-splines or wavelets is not useful, due to the spatially limited segments. Therefore a spatial clustering is carried out in the following.

The measuring points within such a spatial unit are jointly processed with the aim of producing a derived representative per cluster. With this simple definition, spatial clustering is an almost universally usable processing approach, whose computing power is very low, especially if, as in this example, the cluster representative is formed from the mean value.

The definition of the cluster size is realized using the same angle ranges. Thus, in this case 71 clusters are created, which are highlighted in Figure 7 in color. The spatial extent of the clusters vary between 0.1 m and 1.4 m, but the number of measuring points included in every cluster is almost constant. This offers the advantage that the measuring time for all clusters is about the same duration and thus the uncertainty due to the sequential measurement has the same magnitude.

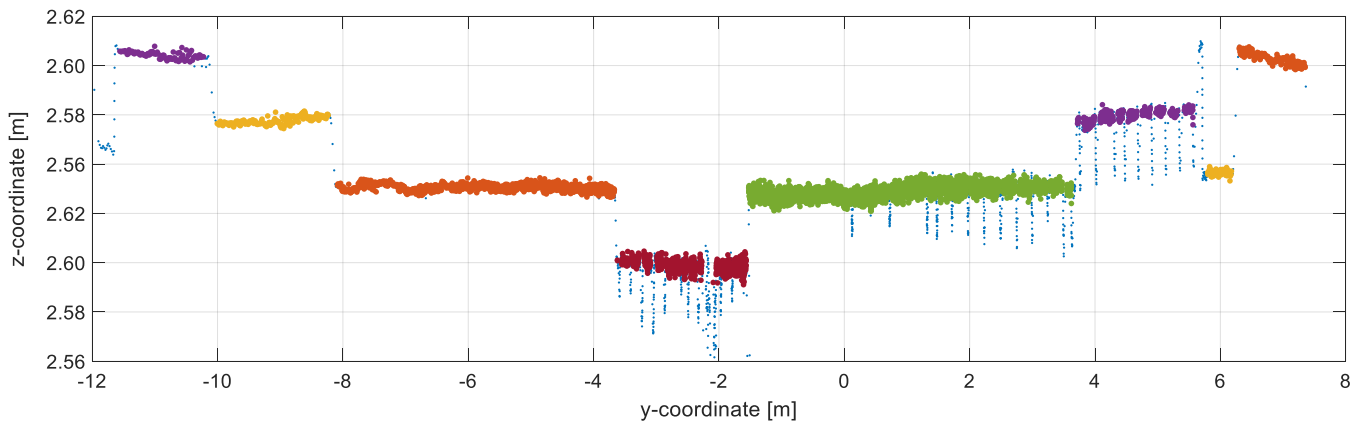


Fig. 6 Automatic segmented measuring profile along a main girder.

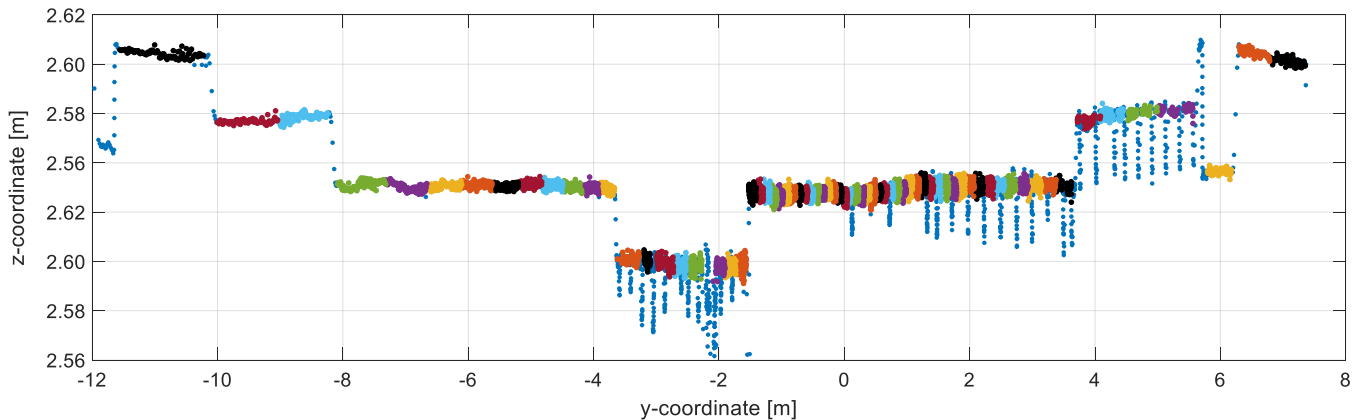


Fig. 7 Spatial clustering based on the automatic segmentation.

By processing the spatially distributed clusters, the transition to a spatio temporal representation is created, see Figure 8. The top chart shows the time series of a cluster representative in the middle of the structure.

In the six diagrams underneath exemplary epochs of the space-time representation are shown on the right side. On the left side, the corresponding position of the train is shown on the bridge. The position at which the time series shown in the top chart was evaluated, is additionally marked with a blue arrow.

The assignment of the cluster representatives within the epochs of the spatial representation (right side) to the bridge structure in Figure 7 is possible on the basis of the consistent coloring of the clusters and their representatives. The temporal mapping of the six spatial representations can be done using the time stamps or the corresponding coloring of the markers in the top chart.

In combination with the situational sketches, the top-level diagram is used to illustrate the general sequence of the train crossing:

The load of the wagons is divided between the two bogies, so that the double wagon shown in this example has four load points, the middle two of which are so close that these two can be combined. The following considerations therefore assume three load points with different loads. Since the distance of the bogies with 17 m is almost as large as the span of the main beams with 19.6 m, there is usually only one load point on the bridge at the same time.

Accordingly, the time series of the z-coordinate of the cluster representative in the upper diagram in Figure 8 shows three local minima. The maximum deflection (middle minimum) occurs when the rear bogie of the first wagon is located on the bridge together with the front bogie of the second wagon (middle load point). The other two local minima are caused by the other bogies of the front or rear wagon.

In the six epochs depicted in Figure 8, the relative changes of the bridge form are illustrated. This shows that the bending line, as expected, takes on a different shape depending on the position of the bogies of the wagons on the bridge:

1. The green epoch shows the situation after the front bogie of the first wagon has been driven onto the bridge. The amplitude of the bending line is low and the shape is asymmetric according to the train position.
2. At the time of the blue epoch, the first bogie of the first wagon is located directly in the middle of the bridge, which at this time is the first local minimum. The shape of the bending line is symmetrical around the center of the bridge with a maximum amplitude of 5 mm.

3. In the turquoise epoch the first partial relief of the bridge is shown. The first and second load points are symmetrical to the center of the bridge at the two bridge edges, which also creates a symmetrical bend line characterized by two load points. An almost constant deflection of 2 mm is achieved over a total area of about 9 m.
4. The black epoch shows the maximum load on the bridge through the central load point (two bogies). The maximum deflection of nearly 8 mm occurs in the middle of the bridge. However, the load situation corresponds to the blue epoch but with a higher load. In the area of the y-coordinate of 3.5 m, some cluster representatives have a greater deflection than would be expected for a homogeneous bend line. This is the border area of the fourth structural segment from the right, compared to Figure 7.
5. The magenta epoch shows a very asymmetrical bending line, since during the double-load point just leaves the bridge, the last bogie is not yet in the middle of the bridge.
6. The time of the red epoch shows the situation just before the last bogie leaves the bridge. The shape of the bending line is similar to a mirrored version of the green epoch.

The spatio temporal processing allows the acquisition of the entire surface structure within a profile. Therefore it is possible to directly measure the complete bending line, and also to detect deviant behavior of individual profile segments, as seen exemplary in the black epoch in Figure 8.

Such model disruptions can be detected with profile scanner measurements, due to the high spatial resolution. In comparison this is not possible with classical sensors for the monitoring of bridges, because the density of the discrete measuring points is much sparser.

Therefore the decision for those discrete measuring positions has to be planned based on appropriate prior knowledge about the supporting structure or on the theoretical deformation behavior.

The usage of profile scanning has the advantage that there is no need for such a great effort for the measuring planning. On the contrary it offers high flexibility combined with low planning expenses.

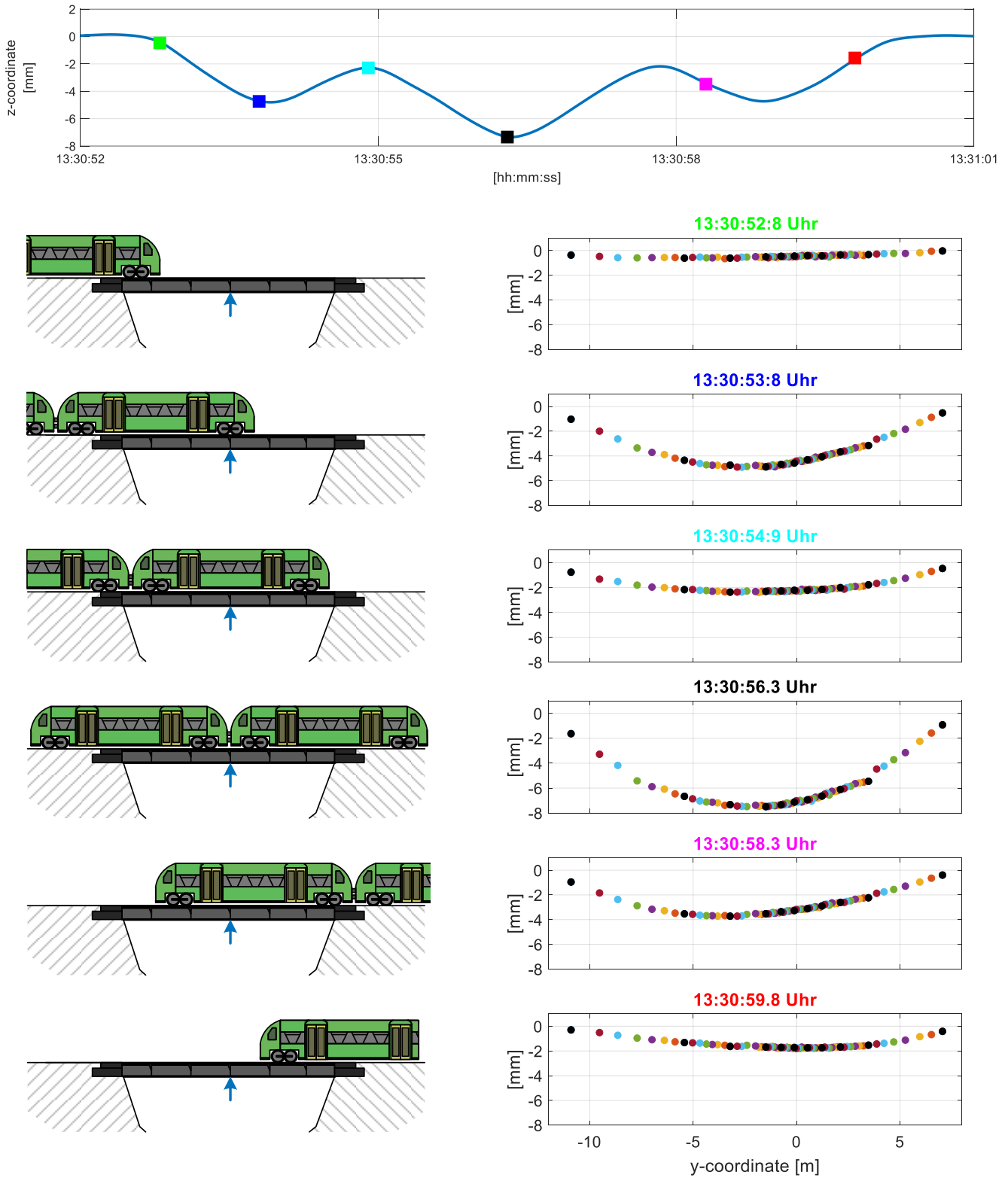


Fig. 8 Spatio temporal representation of a train crossing with two wagons. Top graph: Time series of a cluster representative for the classification of the individual epochs of spatial representation. The remaining six illustrations correspond to the spatial representation of a defined point in time during the crossing (epochs).

4.2 Analysis of the main girders perpendicular to the bridge axis

In addition to the evaluations of the vertical component shown in the previous analyses, the horizontal deformation of the bridge can be recorded in particular with the measurement of the configuration 2. The following versions are therefore concerned with the evaluation of this configuration, which was measured perpendicular to the main bridge axis. The focus lies on the simultaneous recording of the horizontal deformation of both main girders.

The position of the bridge in a curve, creates in addition to the vertical deformation also a horizontal deformation of the main girders. This is caused by the combination of the centrifugal force due to the curve position of the bridge and the sine run of the train [8].

To determine the horizontal deformation, a modified automatic analysis of the measuring profiles must be carried out, wherein the analysis focuses on the y-coordinate values. Based on the resulting segmentation, a spatial clustering takes place, the result of which is shown in Figure 9.

Here, too, the cluster definition takes place over the same angle range, so that all clusters contain approximately the same number of measuring points.

For the determination of the horizontal deformation of the two main girders, the blue cluster is selected on the main girder 1 and the orange cluster on the main girder 2 as representative examples. Both cluster have a vertical extension of approx. 0.15 m and include approximately 80 points.

Figure 10 shows the time series of the cluster representatives of the blue and orange cluster from Figure 9. Both time series are divided into three parts: before the crossing, during the crossing and after the crossing, which are visually separated from each other by black lines.

The uncertainty for the y-coordinate of the two cluster representatives can be determined from the cut-outs before and after the crossing (without load) in the time domain. The blue time series results in a standard deviation of approx. 0.13 mm and the orange time series results in a standard deviation of approx. 0.11 mm.

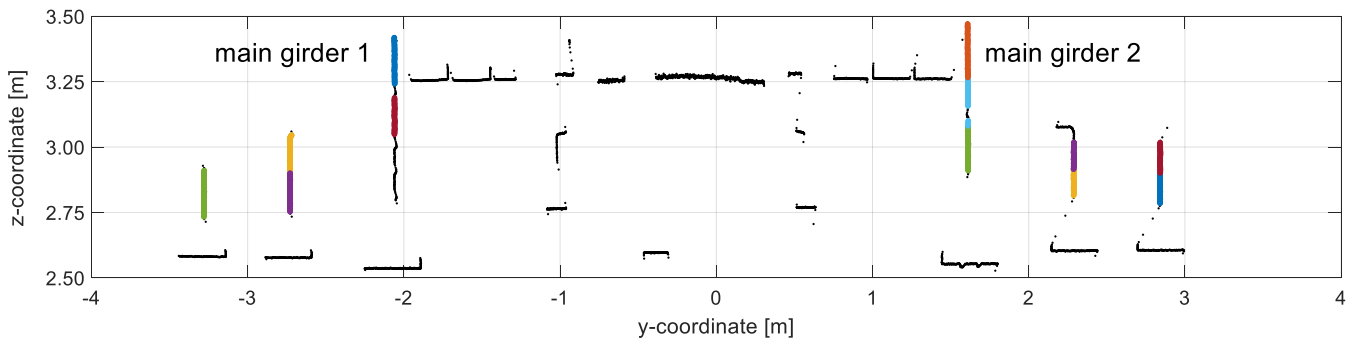


Fig. 9 Spatial clustering based on the automatic segmented profile in configuration 2.

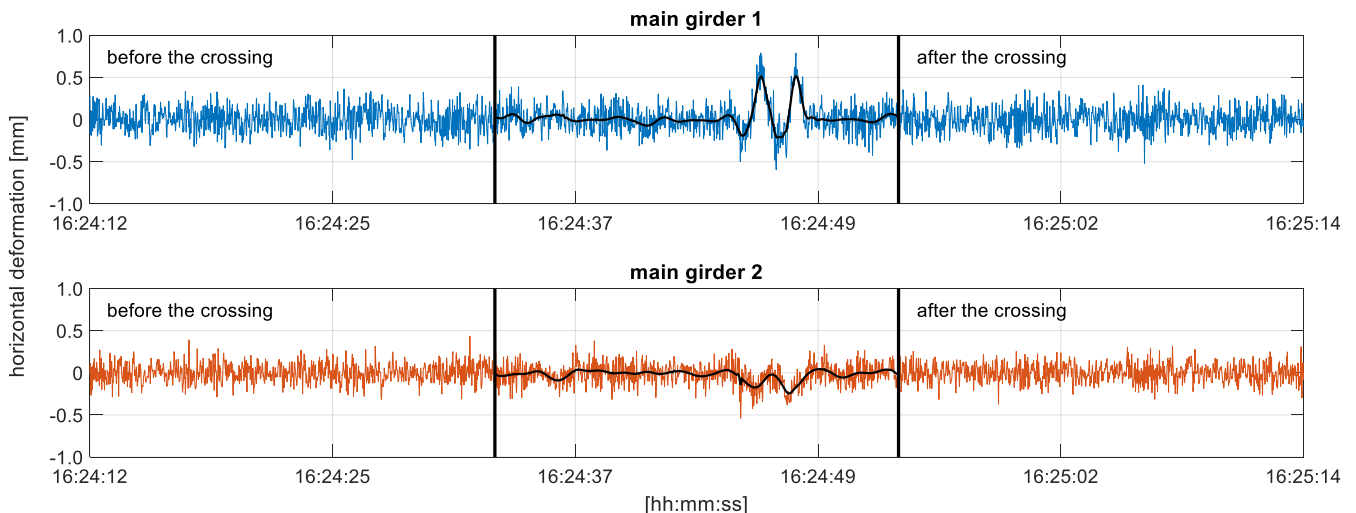


Fig. 10 Time series of the cluster representatives for the blue and orange cluster.

Using these results, the cutout during the crossing is denoised (wavelet denoising) and the result is superimposed on the actual deformation signal in black.

In both time series, the horizontal deformations can be verified which are induced by the forces from the bogies of the train. The main carrier 1 (outside of the curve) has a maximum horizontal deformation of over 0.5 mm at the crossing of both bogies. For the main carrier 2, the magnitude of the horizontal deformation is only just above the noise level. This shows that due to the position in the curve most of the horizontal load rests on the outer track.

Due to the possibility of a combined registration of the vertical (Chapter 4.1) and horizontal deformation of supporting structures, the use of the profile scanner also provides the potential to capture information about the structural behavior in order to improve the planning of large measurement campaigns. For example, it can be preanalyzed whether the lateral deformations of the bridge distorts the results of other sensors culminating in the verification and even correction of the measurements of those sensors, see [9].

5. Example 2: Trough bridge over the Aller

The second monitored engineering structure is a newly built railway bridge over the Aller near Verden (Niedersachsen). The bridge is 380 meters long, consists of seven bridge spans and was executed as a joint less steel bridge. The maximum route speed is 160 km/h.

All measurements took place on the eastern main beam of the bridge in longitudinal direction. The measured bridge span has a length of approx. 50 m, see Figure 11.

In contrast to the single-tracked railway bridge from Chapter 4, the surface of the main beam has no structuring, so that the automatic analysis of the measurement profiles only creates one profile segment.



Fig. 11 Trough bridge over the Aller.

For this reason, all spatial processing methods presented in Chapter 3 are suitable for further analyses.

Figure 12 depicts the results of the spatial clustering and the B-spline approximation for a single measurement profile on the eastern main beam between two supports.

The profile points are divided into 100 spatial clusters and are appropriately colored. The expansion of the spatial cluster is again chosen in such a way that all cluster contain approximately the same number of profile measuring points (approximately 90 points each), which varies the cluster extent between 0.1 m and 4 m.

In addition, a B-spline approximation is superimposed on the measuring points in black. For the theoretical background see e.g. [10], [11] or [3].

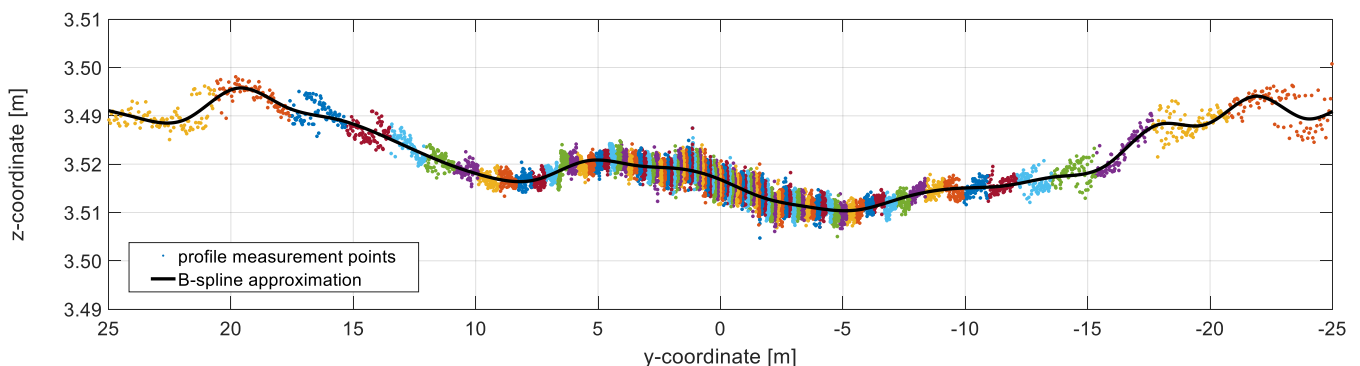


Fig. 12 Results of two processing methods: spatial clustering (colored) and B-spline approximation (black).

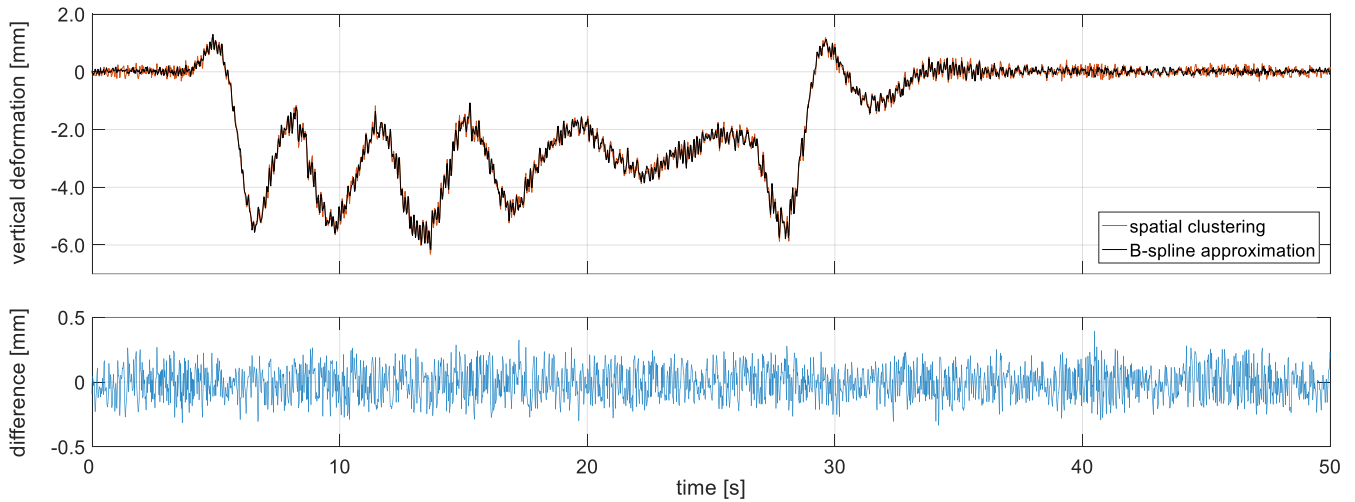


Fig. 13 Time series of the z-coordinates of both processing methods at the y-coordinate -10.39 m and their differences.

In order to compare the results of the two profile-wise spatial processing methods, the same positions on the supporting structure were evaluated. These positions are specified in this case by the representatives of the 100 clusters and were also evaluated with the B-spline approximation. Therefore a total number of 100 time series distributed over the entire structure are available.

In the upper diagram in Figure 13, the time series of the z-coordinates for both processing methods are shown exemplary for one position on the structural member (y-coordinate -10.39 m). It is a 50-second section of the crossing of a freight train, which was recorded with 50 Hz and contains therefore 2.500 measurements.

The lower diagram shows the differences between those two processing methods. Those differences do not contain any systematic effects and are mainly caused by the slightly larger noise level of the spatial clustering. This is why we only look at the results of the profile-wise B-spline approximation in the following.

The time series in the upper diagram of Figure 13 consists primarily of a low-frequency signal component due to the load of the train and a superpositioned high-frequency signal component due to the dynamic excitation of the bogies of the train. In the following, these two parts are called the quasi-static and the dynamic signal component of the time series.

With the use of the multiresolution analysis (MRA) of the discrete wavelet transform for the time series not only noise can be eliminated, but it is also possible to separate frequency ranges. The MRA to be used decomposes the signal into individual frequency bands, see e. g. [12] or [13]. With the wavelet synthesis the wanted signal components can be reconstructed and thus, the transition from the total deformation to the dynamic signal component can be realized, see Figure 14.

In the upper diagram, the black line shows the quasi-static signal component determined by means of wavelet decomposition/synthesis. The time series of the dynamic deformation component is shown in blue in the lower diagram.

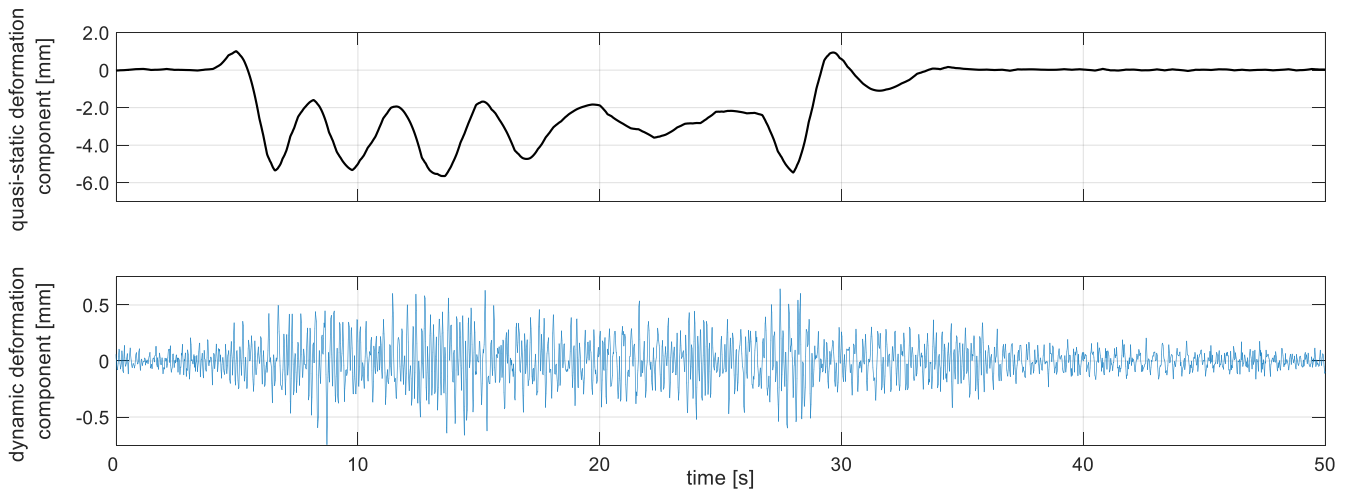


Fig. 14 Separation of the dynamic and quasi-static deformation component of the sample time series from Figure 13.

Based on the separation of the quasi-static from the dynamic deformation component, two selected positions on the structural member are analyzed in the following. These are a position in the middle of the field (y-coordinate: -0.0 m, yellow) and approximately the quarter point (y-coordinate: -10.39 m, purple). These two positions are highlighted in the top chart in Figure 15 with colored dots and also in Figure 16 with colored lines. The choice of these positions is based on the theoretical eigenmodes of a simple beam [14], shown in Figure 16. This simple model can also be a good approximation for simple bridges.

While in the middle of the beam the first eigenmode has its maximum, the second eigenmode has a zero pass. In the quarter point, however, the second eigenmode has its maximum, while the amplitude of the first eigenmode decreases.

In the diagrams shown below in Figure 15, the dynamic deformation components in the time series of the individual positions are shown on the left side and the corresponding amplitude spectra on the right side. For the two positions on the structure, three ranges can be identified in the amplitude spectra, in which frequencies occur above the noise level: approximately at 2-3 Hz, at 5 Hz and at 8 Hz.

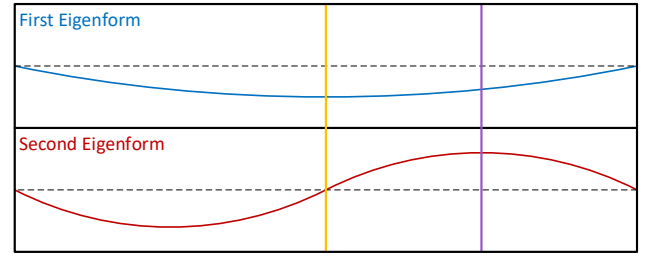


Fig. 16 Theoretical eigenmodes of a beam.

The so far considered time series underlying the amplitude spectra include the train crossing, as well as areas in which the supporting structure is at rest and also the free decay process of the structure. Therefore it is not possible to make a valid statement about the association of those frequency ranges to the natural frequencies. In principle, you can only see that certain frequencies within the time series have occurred at least temporarily.

To avoid this problem we will concentrate on a shorter part of the time series: the free decay process after the train left the monitored bridge span. Due to the high spatial resolution of the profile scanner we can simultaneously widen our view in the context of spatial resolution.

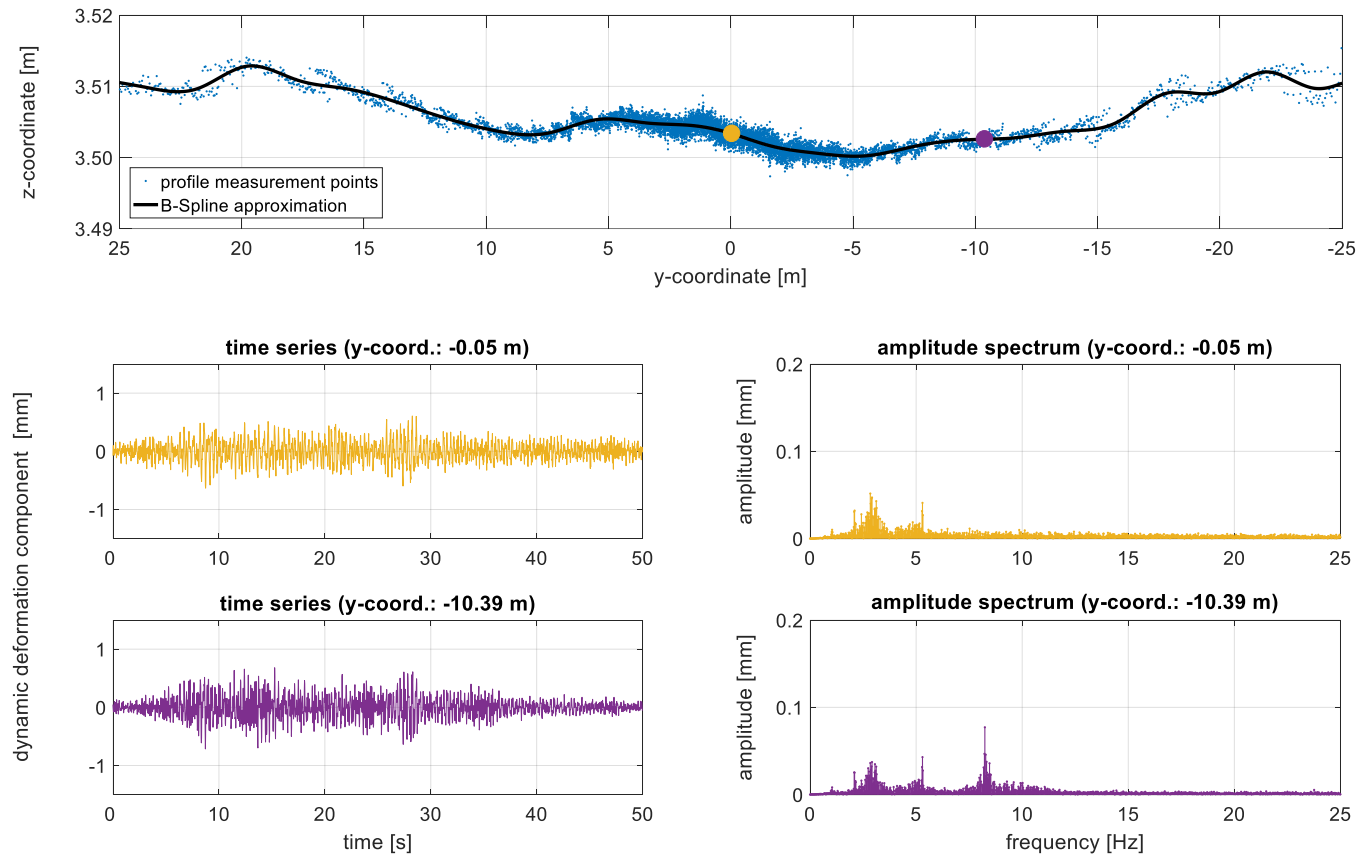


Fig. 15 Dynamic deformation component in the time- and frequency domain at two discrete points of the bridge span.

The two position representation in Figure 15 corresponds to the traditional analysis of classical sensors used for the monitoring of bridges. However, the almost space-continuous detection of the structural surface with the profile scanner can be used to view the entire bridge span in detail, maintaining a temporal resolution of 20 ms, for a corresponding waterfall representation see Figure 17.

On the x-axis the position on the structure is shown, on the y-axis the frequency range (limited to the relevant area up to 12 Hz) and on the z-axis the magnitude of the amplitudes is plotted.

Thus, the free decay process is represented in the frequency domain for the entire bridge span.

In Figure 17 significant amplitudes occur only at the frequencies of 3.1 and 8.3 Hz. The previously occurring amplitudes at 5 Hz and the secondary maxima in the frequency range around 3 Hz are, however, no longer existing, compared with Figure 15.

Hence, it can be concluded that 3.1 Hz is the first natural frequency (eigenfrequency) and 8.3 Hz is the second natural frequency. Since the associated distribution of the amplitude maxima corresponds mostly to the theory as seen in Figure 16.

This is further confirmed by the phase position of the occurring frequencies, which is constant for 3.1 Hz (first natural frequency) over the entire structure, while the phase position for 8.3 Hz (second natural frequency) is symmetrically to the middle of the bridge, but with inverse sign.

However the amplitudes of the likely second eigenmode increase on both sides till the end of the measured bridge span. According to the theory from Figure 15 there should be a decrease in amplitude beginning at the quarter point till the support. This difference between the theory and the profile scanner measurements is likely caused by the too simple model, which does not take the real support conditions and the fact that the bridge consists of seven bridge spans into account.

Those differences can only be evaluated with the high spatial resolution of the profile scanner. Otherwise only measurements at predefined points are carried out in most cases according to the theory, like the graphs depicted in Figure 15.

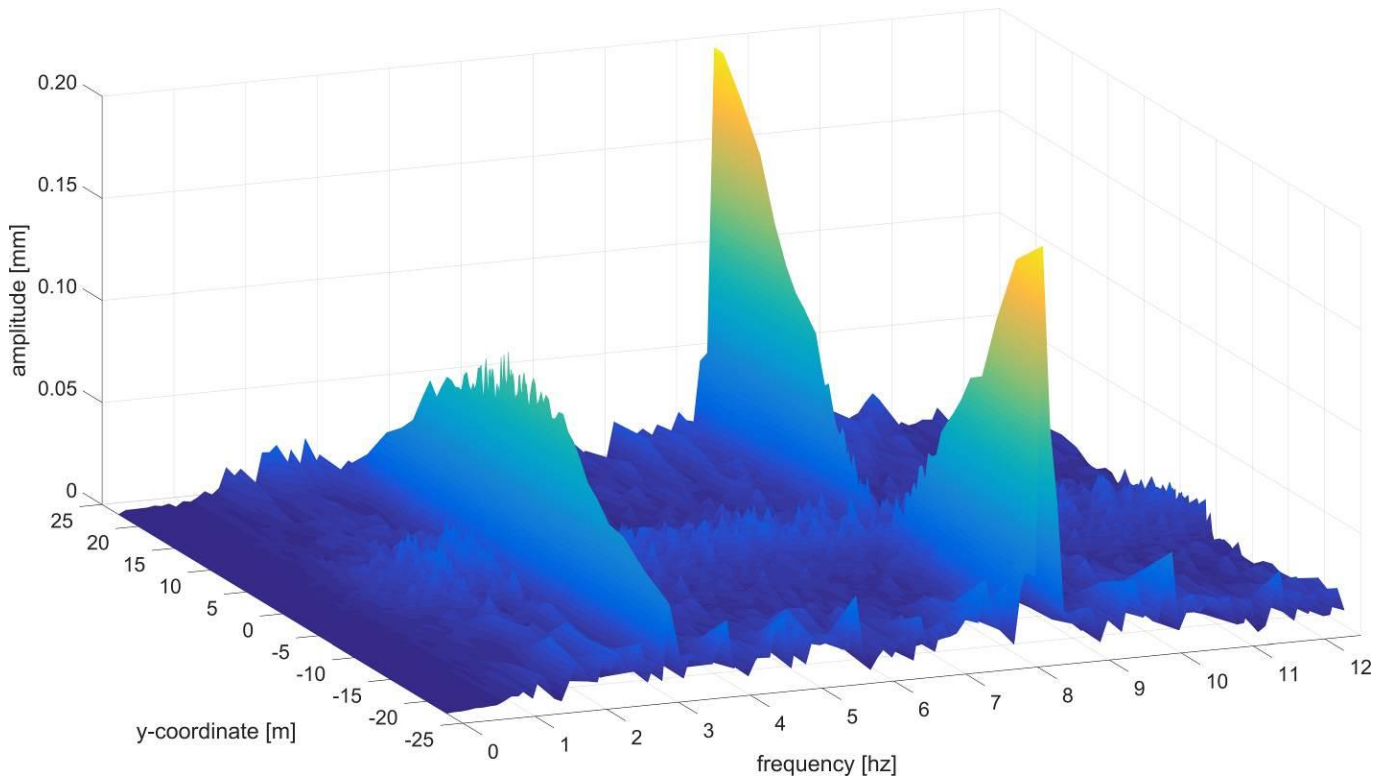


Fig. 17 Amplitude spectra of the dynamic deformation component for the free decay process of the monitored bridge span.

6. Conclusions

Those two examples demonstrate that a non-contact measuring system like a profile scanner can capture temporally variable structural deformations more efficiently and in a much higher spatial resolution than typically used sensors for the monitoring of supporting structures. Furthermore it is possible, with the presented measurement and evaluation methodology, to reach uncertainties of nearly the same scale as generated with classical discrete measurement sensors.

Due to the high spatial and temporal resolution large amounts of data are recorded. For practical use, this implies that the automatically collected data needs a largely automated processing and quality assessment.

With the spatio temporal processed data basis it is possible to derive deformation measurements at nearly any desired position within a supporting structure profile (post mission). Therefore the dependence on prior knowledge about the structure or on the theoretical deformation behavior is greatly reduced. That applies to the measurement planning as well as the analysis of the deformation behavior.

The adaptable spatial resolution furthermore enables the detection of model disruptions or deviant behavior of parts of the supporting structure. Thus, it is possible to verify structure models and to improve their predictive quality accordingly.

References

- [1] Otto Heunecke, Heiner Kuhlmann, Walter Welsch, Andreas Eichhorn and Hans Neuner, Handbuch Ingenieurgeodäsie - Auswertung geodätischer Überwachungsmessungen, Springer-Verlag, ISBN: 9783879074679, 2013
- [2] Zoller + Fröhlich, Z+F PROFILER® 9012 Datasheet, URL: http://www.zf-laser.com/fileadmin/editor/Datenblaetter/Z_F_PROFILER_9012_Datenblatt_D_final_kompr.pdf (visited at 20. 07. 2018), 2018
- [3] Florian Schill, Überwachung von Tragwerken mit Profilsclannern, Dissertation, Technische Universität Darmstadt, Darmstadt, 2018
- [4] Florian Schill and Andreas Eichhorn, Automatische Segmentierung von Profilsclannermessungen am Beispiel von Brückenbauwerken, Ingenieurvermessung 17, Beiträge zum 18. Internationalen Ingenieurvermessungskurs Graz, Graz, 2017
- [5] Carl De Boor. A practical guide to splines. Applied mathematical sciences, Springer-Verlag, ISBN: 9780387953663, 2001
- [6] David L. Donoho and Iain M. Johnstone, Ideal spatial adaptation by wavelet shrinkage, Biometrika 81.3, S. 425–455, 1994
- [7] Florian Schill and Andreas Eichhorn, Investigations of low- and high-frequency movements of wind power plants using a profile laser scanner, 3rd Joint International Symposium on Deformation Monitoring (JISDM), Vienna, 2016
- [8] Jia Liu, Einfluss der Schienenbefestigungskomponenten auf das laterale Verformungs- und Lastverteilungsverhalten der Schiene, Dissertation, Technische Universität München, München, 2011
- [9] Matthias Becker, Birgit Traiser, Florian Schill, Jens Schneider and Andrei Firus, Messung und Identifikation dynamischer Strukturparameter mittels terrestrischer Mikrowelleninterferometrie, Messen im Bauwesen, 2016
- [10] Hans Neuner, Claudius Schmitt and Ingo Neumann, Modelling of terrestrial laser-scanning profile measurements with B-Splines, Proceedings of the 2nd Joint international Symposium on Deformation Monitoring (JISDM), Nottingham, 2013.
- [11] Johannes Bureick, Hamza Alkhatib and Ingo Neumann, Robust Spatial Approximation of Laser Scanner Point Clouds by Means of Free-form Curve Approaches in Deformation Analysis, Journal of Applied Geodesy 10.1, S. 27–35, 2016
- [12] Werner Bäni, Wavelets: Eine Einführung für Ingenieure, Oldenbourg Verlag, ISBN: 9783486594003, 2005
- [13] Donald B. Percival and Andrew T. Walden, Wavelet Methods for Time Series Analysis, Cambridge Series in Statistical and Probabilistic Mathematics. Cambridge University Press, ISBN: 9780521640688, 2000
- [14] Dietmar Gross, Werner Hauger and Peter Wriggers, Technische Mechanik 4: Hydromechanik, Elemente der Höheren Mechanik, Numerische Methoden Springer-Verlag, ISBN: 9783662556948, 2018